Environ Fluid Mech (2017) 17:473–483
DOI 10.1007/s10652-016-9499-3

ORIGINAL ARTICLE

Impact of windage on ocean surface Lagrangian coherent structures

Michael R. Allshouse[1] · Gregory N. Ivey[2] · Ryan J. Lowe[3] · Nicole L. Jones[2] · C. J. Beegle-Krause[4] · Jiangtao Xu[2] · Thomas Peacock[1]

Received: 13 July 2016 / Accepted: 1 December 2016 / Published online: 16 December 2016

Abstract Windage, the additional direct, wind-induced drift of material floating at the free surface of the ocean, plays a crucial role in the surface transport of biological and contaminant material. Lagrangian coherent structures (LCS) uncover the hidden organizing structures that underlie material transport by fluid flows. Despite numerous studies in which LCS ideas have been applied to ocean surface transport scenarios, such as oil spills, debris fields and biological material, there has been no consideration of the influence of windage on LCS. Here we investigate and demonstrate the impact of windage on ocean surface LCS via a case study of the ocean surrounding the UNESCO World Heritage Ningaloo coral reef coast in Western Australia. We demonstrate that the inclusion of windage is necessary when applying LCS to the study of surface transport of any floating material in the ocean.

Keywords Lagrangian coherent structures · Windage · Ningaloo

Electronic supplementary material The online version of this article (doi:10.1007/s10652-016-9499-3) contains supplementary material, which is available to authorized users.

✉ Michael R. Allshouse
allshouse@mit.edu

[1] ENDLab, Department of Mechanical Engineering, Massachusetts Institute of Technology, Cambridge, MA, USA

[2] School of Civil, Environmental and Mining Engineering & Oceans Institute, University of Western Australia, Crawley, Australia

[3] School of Earth and Environment & Oceans Institute, University of Western Australia, Crawley, Australia

[4] Materials and Chemistry/Environmental Modeling, SINTEF, Trondheim, Norway

1 Introduction

Ocean surface transport lies at the heart of a panoply of natural and human-induced scenarios, including marine population connectivity [6], iceberg drift [24], the spreading of oil slicks [1] and search-and-rescue planning [4]. For a variety of different physical reasons, however, material floating on the ocean surface does not travel with the velocity of the surface layer of the ocean. Material that has inertia, for example, has a velocity relative to the surrounding fluid due to the history of forcing [19]. Another factor is the impact of windage, representing the additional drag force on, and hence motion of, floating material due to the direct exposure to wind forcing at the ocean surface. Windage is known to substantially influence the fate of reproductive biological material that affects ecological connectivity [20, 23] as well as anthropogenic releases such as oil spills [1, 17] and floating debris [4].

The Lagrangian coherent structure (LCS) approach has been at the forefront of a new perspective on understanding material transport in the ocean [2, 14, 28]. This approach uses a time history of velocity field data, obtained from either numerical models or coastal high frequency (HF) radar stations [1, 5], to identify key repelling and attracting material lines that, as they are advected and deformed by the flow, play a central role in directing material transport. Generally not evident in snapshots of the (Eulerian) velocity field, these material lines are commonly referred to as the skeleton that underlies flow transport [18]. LCS analysis has been applied to a wide variety of ocean flows [14, 30] and two key concepts that have emerged are those of principal strainlines [7] and hyperbolic cores [26]. Principal strainlines are the strongest normally-repelling material lines (i.e. in a direction perpendicular to the material line) for the time window and domain considered. A hyperbolic core is the point on the strongest attracting strainlines that is persistently hyperbolic and has the ability to predict imminent transport events. One of the most attractive features of the LCS analysis is its robustness to noise in the velocity field [12].

Because floating material does not necessarily move with the ocean surface layer, relevant LCS analysis must account for this modified transport. LCS analysis has been extended to account for inertia [13]. A key result is that elliptic LCS, representing Lagrangian vortices, trap inertial material in their midst, providing the rationale for the focusing of chlorophyll in eddies [3]. Despite the fact that windage is known to influence the fate of floating material, all previous studies that apply LCS methods to ocean surface transport scenarios, such as oil spills (e.g. [21] and [26]), do not account for windage. Since windage impacts the trajectories of floating objects, understanding the structure of material transport at the ocean surface through LCS analysis that incorporates how windage changes the effective velocity field is the focus of this study.

For our case study, we consider a particular geographic setting where the confluence of oceanography, environmental considerations and offshore engineering development make surface transport a topic of keen interest, and where surface winds are known to be variable and play a central role in the ocean dynamics. The UNESCO World Heritage Ningaloo Reef is a 300 km long fringing coral reef in Western Australia (Fig. 1a and inset Fig. 1c). The shelf circulation off the Ningaloo Reef is characterized by complex interactions between the southward flowing offshore Leeuwin current, local wind-driven currents, and transient mesoscale features in the region. Driven by a strong and persistent poleward pressure gradient, the offshore, along-shelf poleward flowing Leeuwin current consolidates south of the North West Cape and accelerates southward down the coast [10, 32]. The along-shore currents on the inner-shelf are only weakly influenced by the offshore Leeuwin

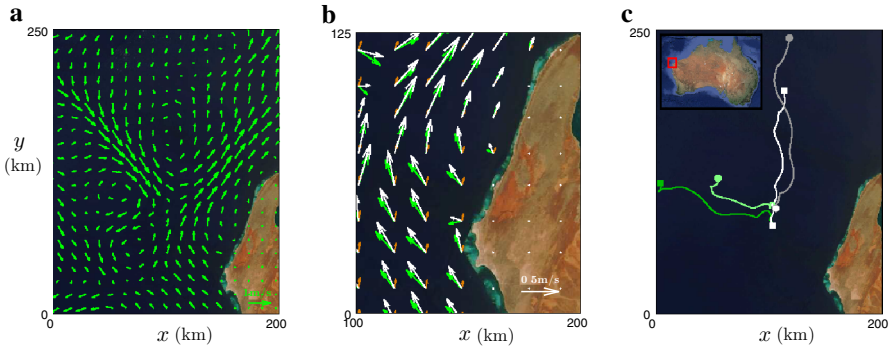

Fig. 1 Velocity and windage fields for the region offshore of Ningaloo reef (see *inset* in **c** for location of Ningaloo in northwestern Australia). **a** Snapshot of the instantaneous surface layer velocity field at 0:00 11 December 2009. **b** Zoomed in snapshot of the surface layer velocity field (*green arrows*), the windage field using a windage factor of $C_w = 0.015$ (*orange arrows*), and the hybrid transport velocity field (*white arrows*). **c** Particle paths over a seven day time window for a pair of particles initially released close together without (*light/dark green*) and with (*white/light gray*) windage. (see SM1 in Supplementary Information for an animated version of these results. Background image from Global Ocean Associates/NASA)

current, but are strongly influenced by the local wind forcing [16, 35, 36]. The winds in the region are predominately variable in speed and direction, but week-long strong persistent southwesterly winds can arise in the spring and early-summer (October–January) resulting in near-coast upwelling-favorable conditions.

This paper proceeds, in Sect. 2, with a discussion of the LCS approach incorporating windage. In Sect. 3, we describe the field data validated simulation of the Ningaloo region and then apply our LCS analysis to two different time windows from the simulation, in both cases comparing and contrasting results with and without windage. The impact of windage on the LCS and the resulting implications are discussed in Sect. 4.

2 Methods

2.1 LCS analysis

Utilizing simulated or high frequency radar velocity fields, one can perform an LCS based analysis [14] of the surface flow. First, the flow map, $\boldsymbol{F}_{t_0}^{t_1}(\boldsymbol{x}_0)$ is calculated, by advecting passive tracers from their initial position, $\boldsymbol{x}_0$ at time t_0, to their final position $\boldsymbol{x}$ at time t_1. The gradient of the flow map can then be used to calculate the Cauchy–Green deformation tensor $\boldsymbol{C}_{t_0}^{t}(\boldsymbol{x}_0)$, which measures the local deformations near a given trajectory over the time interval. The eigenvalues and eigenvectors of this tensor correspond to the magnitudes and directions of greatest and least stretching. More specifically, material lines tangent to the eigenvectors corresponding to the smaller eigenvalues have inherently strong normal repulsion; of these material lines, the ones that contain the maximum larger eigenvalues are considered to be particularly pertinent transport features, and are referred to as strainlines. This analysis is valid for both incompressible and compressible systems as in both cases the eigenvectors of the Cauchy–Green deformation tensor are orthogonal. While it is possible in a compressible system to have both eigenvalues be less than (or greater than)

unity, corresponding to local contraction (or expansion), we will consider only strainlines that are everywhere normally repelling, i.e. the larger eigenvalue is greater than unity.

Because the LCS procedure can be implemented both forward (i.e. t_0 to t_1) and backward (i.e. t_1 to t_0) in time, one can also identify strainlines that are maximally repelling in backwards time, these being maximally attracting in forwards time. For this reason, we refer to forwards-time strainlines as repelling and backwards-time strainlines as attracting. A subtle, but important, point is that the calculation of the repelling and attracting strainlines over the same time interval is necessary in order to have a kinematically consistent representation of the system transport. By the nature of their calculation, however, the form of repelling strainlines is obtained at the initial time t_0, while the form of the attracting strainlines is obtained at the final time t_1.

Farazmand and Haller [8] produce a kinematically consistent representation of strainlines, which they referred to as stretch and shrinklines, by calculating the vector lines from the singularity points in the eigenvalue field. Due to the sensitivity of the singularity point in our analysis, we obtain complementary sets of strainlines at any time instant through advection of the calculated repelling and attracting strainlines. The advection of attracting and repelling strainlines is difficult because the repelling and attracting strainlines are highly repulsive when advected forward and backwards in time, respectively, and so any initially small error grows dramatically with advection. To overcome this challenge, we recursively calculate the strainlines from a given eigenvector field, identifying the strongest repelling structure, improving the resolution of the eigenvector field in that region, and repeating the process, which enabled the smooth advection of these sensitive material lines. Had the surface velocity field been incompressible, it would have been possible to apply the method developed by [15].

By advecting the strainlines to the same time instant, it is possible to identify where repelling and attracting strainlines intersect. We refer to such intersections as Lagrangian hyperbolic saddle-points because the flow near these points is similar to a saddle-point flow, presented in the inset in Fig. 2a. We note that while the concept of a Lagrangian

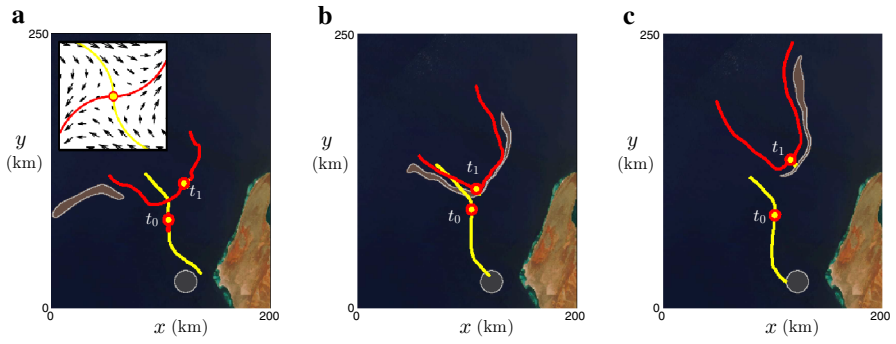

Fig. 2 The impact of windage on a hypothetical tracer release event off Ningaloo Reef between 0:00 11 December 2009 (t_0) and 0:00 18 December 2009 (t_1). **a** In the absence of windage, the initially circular tracer patch (*gray patch*) and the dominant Lagrangian hyperbolic saddle-point (*red/yellow circle*) are advected from time t_0 to time t_1. In its final state, the tracer patch (*brown patch*) is only modestly stretched by the saddle point because it lies somewhat beyond its domain of influence. The *inset* in **a** presents the local velocity field in the frame of reference of the moving saddle point at an intermediate time, revealing the saddle point like velocity field. The inclusion of windage factors **b** $C_w = 0.0075$ and **c** $C_w = 0.015$ relocates the saddle point, the repelling strainline position relative to the initial tracer patch, and the final patch position. (see SM2 in Supplementary Information for an animated version of these results)

hyperbolic saddle-point is similar to that of a hyperbolic core, introduced by [26], in that it identifies strong hyperbolic behavior, there are two differences: (i) a Lagrangian hyperbolic saddle-point does not require persistent hyperbolic behavior, but (ii) it identifies the strongest repelling and attracting structure as opposed to just the strongest attracting structure. The Lagrangian saddle-point is the first structure to consider both forward and backward-time strainlines in a dynamically consistent way. Mathur et al. [18] identified hyperbolic regions as the intersection of forward and backward time finite-time Lyapunov exponent ridges; however, the repelling and attracting structures were calculated for different time intervals, $[t_0, t_0 + T]$ and $[t_0, t_0 - T]$, respectively.

2.2 Windage

While LCS analysis has been previously applied to ocean surface simulation outputs [14, 30], here we account for the additional impact of wind on transport at the water surface itself, and assess how this affects the dominant transport structures. It is to be expected that windage will play a significant role in the form of ocean surface LCS as it is known that windage impacts trajectories of floating objects, but this has never been previously demonstrated or quantified for LCS despite the methods being widely applied to ocean surface transport problems. In a study on the use of approximate velocity fields, Haller determined that changes to the velocity field that are isolated in space and time do not significantly change the LCS. Even in the presence of persistent stochastic noise, the structures are not effected [12]. However, by persistently changing the velocity field by incorporating windage, we will no longer satisfy the criterion necessary for the structures to remain unchanged.

There are several aspects of windage to consider, but the two dominant considerations are firstly, the relative orientation of surface and windage velocity fields and secondly, that different materials floating at the surface have different windage factors, depending on their size, degree of aerial exposure and other physical attributes. For our studies, we employ the widely-used, empirical model for the hybrid surface velocity $\mathbf{u}(\mathbf{x}, t)$ [1, 9, 17, 22, 29]:

$$\mathbf{u}(\mathbf{x}, t) = \mathbf{u}_c(\mathbf{x}, t) + C_w \mathbf{u}_w(\mathbf{x}, t), \tag{1}$$

where $\mathbf{u}_c$ is the velocity of the ocean surface layer, by convention $\mathbf{u}_w$ is taken to be the wind velocity 10 m above the surface, and C_w is the windage coefficient, which tends to be in the range $C_w = 0.010$–0.044 depending on the material [1, 9, 17, 29]. Models with both constant and variable drift angles in the range 0° to 20° relative to the wind forcing have also been used [31, 34]. For floating debris, or natural floating material such as icebergs, different along- and across-wind components are often utilized, depending on the object shape; this is referred to as leeway drift and there have been detailed studies for ocean drifters [25, 4] as well as many other types of floating objects [4]. If the influence of surface wave transport is also significant, the effect of wave-induced stokes drift can be linearly added to Eq. (1) [1]. Here, as a proof of concept, we use Eq. (1) as a simple but reasonable model of windage. While more complex windage models exist, and indeed different windage models are appropriate to different scenarios, for robust LCS these models will produce different shifts in the position and strength of the structure. It is necessary to incorporate the appropriate windage model in order to identify the fundamental transport structures for the given scenario. In proceeding, we note that the analysis of the hybrid velocity field must be applied across the entire spacial and temporal domain, and not just subsets of this data in order to identify dominant, wind-influenced LCS.

3 Results

We analyzed the 3 month model simulation for the Ningaloo region, from 1 November 2009 to 31 January 2010 produced by [36]. During the austral spring and early summer period, the wind field in the region varies with a time scale of one-to-two weeks: the average wind speed is around 6 m/s, and it is predominantly ($\sim$85% of the time) directed towards the north or northeast and along the coast, and hence is upwelling favorable [16, 35]. During these periods, there is a general offshore-directed flow in the surface layers [35, 36]. In Fig. 1a, we show a typical surface layer velocity field from a period with winds towards the north. Figure 1b presents a snapshot of the corresponding 10 m wind velocity field, and the inclusion of a modest windage factor $C_w = 0.015$ leads to a hybrid transport velocity field from Eq (1) that is notably different from the basic velocity field. A consequence of this inclusion of windage is that the seven day trajectory of particles at the free surface are substantially altered, both in terms of their direction and the amount of stretching or separation between initially adjacent particle pairs (Fig. 1c and SM1 in Supplementary Information). It is therefore to be expected that this will notably impact the LCS results.

LCS analysis was performed for two time intervals; the first interval being 0:00 11 December 2009–0:00 18 December 2009. In the absence of windage, at initial time t_0, the prevailing transport structure is a Lagrangian hyperbolic saddle-point located $\sim$50 km offshore to the west (Fig. 2a). This structure is a generalization of the classic saddle-point structure of dynamical systems theory, illustrated in the inset of Fig. 2a. Because the saddle-point flow is observed in the Lagrangian frame, it is not known *a priori* based on the velocity field alone. As this feature is advected over the time window of interest to time t_1 (see SM2 in Supplementary Information), the repelling strainline contracts to become almost a point on the expanded attracting strainline; this evolution is characteristic of the transport properties of a hyperbolic saddle-point. To demonstrate the influence of the saddle point, we consider a hypothetical tracer release event, be it natural (e.g., algal bloom) or anthropogenic (e.g., oil spill), $\sim$25 km off the Ningaloo coast. The influence of the saddle point is to draw the material further west, away from the coastline, and spread it out over a distance of $\sim$75 km in roughly an east-west direction.

As seen in Fig. 2b, c, the inclusion of windage factors of $C_w = 0.0075$ and $C_w = 0.015$, respectively, which are reasonable factors for natural or anthropogenic material, notably impacts the exact location of the saddle point and the form of the associated attracting and repelling strainlines uncovered by the LCS analysis; the basic structure itself persists, however, as saddle points in dynamical systems are structurally stable in the face of perturbations to the data [11]. For $C_w = 0.0075$ (Fig. 2b), the initial position of the saddle point shifts slightly to the north and, more significantly, the associated repelling strainline shifts south, experiencing a modest change in form and bisects the material patch. These changes have a profound impact on the fate of the material, as after advection to time t_1 the material is greatly stretched by the influence of the saddle point. Although still well offshore, away from the coral reef, the material patch is now spread out over more than 100 km. Increasing the windage factor to $C_w = 0.015$ (Fig. 2c) does not noticeably influence the initial position of the saddle point, but now the initial material release is east of the attracting strainline, and so upon advection the patch is stretched far to the east of the saddle point, in a predominantly northerly direction, to a location $\sim$100 km east of the zero windage result.

There is notable temporal variability in the wind field in the vicinity of Ningaloo and, coupled with the presence of large-scale alongshore pressure gradients, and strong ocean density stratification effects, the actual flow fields are more complicated than predicted by localized simple Ekman layer dynamics [35, 36]. For approximately 15% of the time, the local wind has a component directed towards the south, and is hence downwelling favorable, in turn inducing a flow in the surface layers towards the coast. To investigate this regime, we considered a second interval from 0:00, 21 December 2009 to 12:00, 25 December 2009 when the wind is blowing towards the south. The snapshot of the velocity field in Fig. 3a reveals a complex flow field with a predominantly north–northeast surface layer current of characteristic magnitude 0.5 m/s (reflecting the history of the forcing prior to this day). The surface wind now comes primarily from the northwest with a characteristic magnitude of 7.5 m/s, and inclusion of a modest windage factor $C_w = 0.015$ leads to a hybrid transport velocity field that is directed towards the Ningaloo coastline and quite distinct from the underlying surface layer current (Fig . 3b). Particle paths are now towards the coast but still highly dependent on the presence of windage (Fig. 3c and SM3 in Supplementary Information).

Applying the LCS analysis, firstly in the absence of windage, at initial time t_0 we again find a Lagrangian hyperbolic saddle-point is the prevailing transport feature for the region. In this case the saddle point is only $\sim$25 km offshore to the west (Fig. 4a). As this feature is advected over the time window of interest to time t_1 (see SM4 in Supplementary Information), the repelling strainline contracts to become almost a point on the expanded attracting strainline and the structure ends up $\sim$20 km off the coast to the north. In the absence of windage, therefore, a release event occurring in the southwest is advected north and somewhat further offshore from its initial location, ending up $\sim$30 km from the attracting LCS, which does not significantly impact the patch because it initially lies outside the domain of influence of the LCS.

The inclusion of appropriate levels of windage again impacts the location of the saddle point uncovered by the LCS analysis. Figure 4b, c present results for windage factors of $C_w = 0.0075$ and $C_w = 0.015$, respectively. With increasing windage, the initial location of the Lagrangian hyperbolic saddle-point shifts towards the location of the release event,

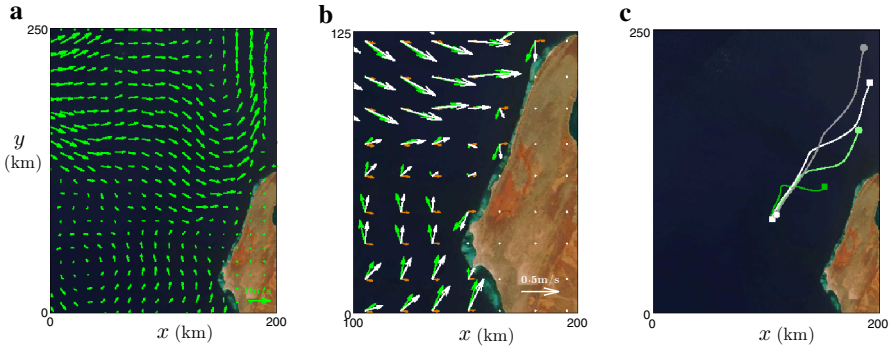

Fig. 3 Velocity and windage fields for the Ningaloo coral reef system. **a** Snapshot of the surface layer velocity field in the vicinity of the Ningaloo reef at 4:00 25 December 2009. **b** Zoomed in snapshot of the surface layer velocity field (*green arrows*), the windage field using a windage factor of $C_w = 0.015$ (*orange arrows*), and the hybrid transport velocity field (*white arrows*). **c** Particle paths over a four-and-a-half day time window for a pair of particles initially released close together without (*light/dark green*) and with (*white/light gray*) windage. (see SM3 in Supplementary Information for an animated version of these results.

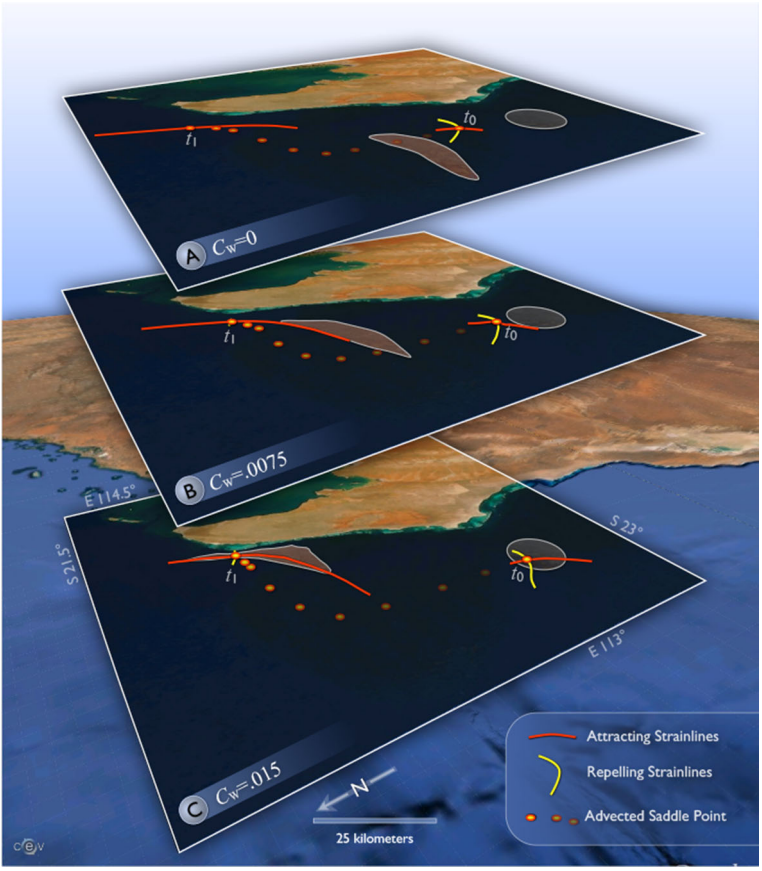

Fig. 4 The impact of windage on a hypothetical tracer release event off Ningaloo Reef between 0:00 21 December 2009 (t_0) and 12:00 25 December 2009 (t_1). **a** In the absence of windage, the tracers (*gray patch*) and the dominant Lagrangian hyperbolic saddle-point are advected along the coastline from time t_0 to time t_1. The final state of the tracer patch (*brown*) is not aligned with the saddle point because it lies beyond its domain of attraction. The position of the saddle point at 12 h intervals between initial time t_0 and final time t_1 is indicated. Inclusion of windage factors **b** C_w = 0.0075 and **c** C_w = 0.015 relocates the saddle point toward the initial tracer patch, causing the tracer patch to be influenced by the LCS and travel along with the saddle point, ultimately being stretched along, and pushed onto, the coastline. (see SM4 in Supplementary Information for an animated version of these results. Image created by CEV.)

thus having increasing influence on the patch's evolution. For $C_w = 0.0075$, the saddle point is initially closer to the patch, which therefore feels the proximity of the attracting strainline as both are advected, and the patch ends up now greatly stretched and in closer proximity to the Ningaloo coastline than in the absence of any windage. For $C_w = 0.015$, the saddle point initially lies within the patch and so the patch is actually pinned to the material point that lies at the intersection of the attracting and repelling strainline. As it is advected (see SM4 in Supplementary Information), the patch is compressed along the orientation of the repelling strainline, which again contracts to a point, and is stretched along the expanding attracting strainline. Furthermore, the saddle- point is now advected further, to be adjacent to the coastline, resulting in direct contact of the material patch with the northern region of Ningaloo Reef.

4 Discussion

Our results provide the first demonstration of the impact of windage on ocean surface LCS. This impact is manifest in the different fates of the material patches in our case studies, which is primarily due to windage influencing the initial position of the patch relative to the position of a Lagrangian hyperbolic saddle-point, and influencing the form of the attracting and repelling strainlines that intersect at the saddle-point. The Lagrangian hyperbolic saddle-point, the identification of which requires advection of strainlines, is a particularly strong reorganization center within the flow and this explains its robustness to the inclusion of different degrees of windage. The observed impact of windage is therefore not to create or destroy such a structure, but rather to affect its position and the arrangement of its attracting and repelling strainlines, and it is this shifting and reshaping that is vital to interpreting the system's advection properties in terms of LCS. It is possible that there are situations where windage is so strong that it eliminates the structures identified from a surface current analysis. Equally, there may be cases where the material is not strongly impacted by windage and the surface current analysis is sufficient. Without properly accounting for the windage the impact can not be known a priori. As such, we conclude that in addition to accepted models of inertia that influence LCS [13], windage should be accounted for in realistic applications of LCS analysis to ocean surface transport.

The role that windage plays is markedly different to that of dispersion as there is spatial and temporal coherence to the additional windage field whereas dispersion is more akin to white noise that impacts trajectories in a spatiotemporally random way. Ultimately, the accuracy of the implementation of windage is only as good as the accuracy of the input surface layer velocity and wind field data sets available. Our consideration of a range of appropriate windage values is an example of the type of investigation needed to assess the confidence with which LCS analysis can be implemented. From our study, for example, we see that there is a persistent LCS feature, a Lagrangian saddle-point, but a variation in the windage value from 0.0075 to 0.015 is the difference between an LCS drawing material onto the shoreline or not.

Obtaining high quality data regarding the ocean surface velocity field and the near surface wind field remains a challenge in the pursuit to understand ocean surface transport. This windage based LCS method could aid management decisions in the coastal ocean, ports and estuaries, which are all locations with strong anthropogenic influences, by providing new understanding of the key underlying flow transport structures. And in regard to Ningaloo, we demonstrate that conditions can exist in which it is possible for dominant Lagrangian transport structures to draw offshore material onto the reef. A next step in the development in this technique would be to identify a Lagrangian saddle-point from measured data, and potentially observe the impact of windage by performing a field test with objects of varying windages. Such a study would build off previous investigations that observed the relationship between coherent structures and drifter advection in the ocean [27] and the influence of winds on surface drifters relative to numerical trajectories [33]. Ultimately, a goal is to set up a near real time LCS monitoring system, incorporating a numerical model, high-frequency radar, and other in situ measurements of ocean and wind data, to monitor and classify the transport conditions for this and other environmentally sensitive coastal regions.

Acknowledgements Simulation data and LCS codes are available upon request to MRA. TP and MRA acknowledge funding support from ONR grant N000141210665. Additional support was provided by the MIT MISTI Global Fund and a UWA Gledden Fellowship. GI, NJ and RL acknowledge support from an

Australian Research Council (ARC) Discovery Project Grant (DP120103036) and RJ from an ARC Future Fellowship Grant (FT110100201).

References

1. Abascal AJ, Castanedo S, Medina R, Losada IJ, Alvarez-Fanjul E (2009) Application of HF radar currents to oil spill modeling. Mar Pollut Bull 58:238–248
2. Allshouse MR, Peacock T (2015) Lagrangian based methods for coherent structure detection. Chaos. 25:097617
3. Beron-Vera FJ, Wang Y, Olascoaga MJ, Goni GJ, Haller G (2013) Objective detection of oceanic eddies and the Agulhas leakage. J Phys Oceanogr 43:1426–1438
4. Breivik O, Allen AA, Maisondieu C, Roth JC (2011) Wind-induced drift of objects at sea: The leeway field method. Appl Ocean Res 33:100–109
5. Coulliette C, Lekien F, Paduano J, Haller G, Marsden J (2007) Optimal pollution mitigation in Monterey Bay based on coastal radar data and nonlinear dynamics. Env Sci Tech 41:6562–6572
6. Cowen RK, Sponaugle S (2009) Larval dispersal and marine population connectivity. Annu Rev Mar Sci 1:443–466
7. Farazmand M, Haller G (2012) Computing Lagrangian coherent structures from their variational theory. CHAOS 22(1):013128
8. Farazmand M, Haller G (2013) Attracting and repelling Lagrangian coherent structures from a single computation. CHAOS 23:023101
9. Galt JA (1994) Trajectory analysis for oil spills. J Adv Mar Tech Conf 11:91–126
10. Godfrey JS, Ridgway KR (1985) The large-scale environment of the poleward-flowing Leeuwin Current, Western Australia: longshore steric height gradients, wind stresses and geostrophic flow. J Phys Oceanogr 15:481–495
11. Guckenheimer J, Holmes P (1983) Nonlinear oscillations, dynamical systems and bifurcations of vector fields. Springer, New York
12. Haller G (2002) Lagrangian coherent structures from approximate velocity field data. Phys Fluids A 14(6):1851–1861
13. Haller G, Sapsis T (2008) Where do inertial particles go in fluid flows? Phys D 237:573–583
14. Haller G (2015) Lagrangian coherent structures. Ann Rev Fluid Mech 47:137–161
15. Karrasch D, Farazmand M, Haller G (2015) Attraction-based computation of hyperbolic Lagrangian coherent structures. J Comput Dynamics 2:83–93
16. Lowe R, Ivey GN, Brinkman RM, Jones NL (2012) Seasonal circulation and temperature variability near the North West Cape of Australia. J Geophys Res Oceans 117:C04010
17. MacFadyen A, Watabayashi GY, Barker CH, Beegle-Krause CJ (2011) Tactical modeling of surface oil transport during the deepwater horizon spill response. Geophys Monog Ser 195:167–178
18. Mathur M, Haller G, Peacock T, Ruppert-Felsot JE, Swinney HL (2007) Uncovering the Lagrangian skeleton of turbulence. Phys Rev Lett 98:144502
19. Maxey MR, Riley JJ (1983) Equation of motion for a small rigid sphere in a nonuniform flow. Phys Fluids 26:883–889
20. McMahon K et al (2014) The movement ecology of seagrasses. Proc R Soc B 281:20140878
21. Mezic I, Loire S, Fonoberov VA, Hogan P (2010) A new mixing diagnostic and Gulf oil spill movement. Science. 330:486–489
22. Ruiz-Montoya L, Lowe RJ, van Niel K, Kendrick G (2012) The role of hydrodynamics on seed dispersal in seagrasses. Limnol Oceanogr 57:1257–1265
23. Ruiz-Montoya L, Lowe RJ, Kendrick G (2015) Contemporary connectivity is sustained by wind- and current-driven seed dispersal among seagrass meadows. Mov Ecol 3:1–14
24. Mountain DG (1980) On predicting iceberg drift. Cold Reg. Sci Tech 1:273–282
25. Niller PP, Davis RE, White HJ (1987) Water-following characteristics of a mixed layer drifter. Deep Sea Res A 34:1867–1881
26. Olascoaga MJ, Haller G (2012) Forecasting sudden changes in environmental contamination patterns. Proc Natl Acad Sci 109:4738–4743
27. Olascoaga MJ et al (2013) Drifter motion in the Gulf of Mexico constrained by altimetric Lagrangian coherent structures. Geophys Res Oceans 40:61716175
28. Peacock T, Haller G (2013) Lagrangian coherent structures: The hidden skeleton of fluid flows. Phys Today 66:41–47

29. Reed M, Turner C, Odulo A (1994) The role of wind and emulsification in modelling oil spill and surface drifter trajectories. Spill Sci Tech Bull 1:143–157
30. Samelson RM (2013) Lagrangian motion, coherent structures, and lines of persistent material strain. Ann Rev Mar Sci 5:137–163
31. Samuels WB, Huang NE, Amstutz DE (1982) An oil spill trajectory analysis model with a variable wind deflection angle. J Ocean Eng 9:347–360
32. Smith RL, Huyer A, Godfrey JS, Church JA (1991) The Leeuwin current off Western Australia, 1986-1987. J Phys Oceanogr 21:323–345
33. Sturges W, Bozec A (2013) A puzzling disagreement between observations and numerical models in the central Gulf of Mexico. J Phys Oceanogr. 43:2673–2681
34. Spaulding ML (1988) A state-of-the-art review of oil spill trajectory and fate modeling. Oil Chem Poll 4:39–55
35. Xu J et al (2013) Dynamics of the summer shelf circulation and transient upwelling off Ningaloo Reef, Western Australia. J Geophys Res Oceans 118:1–27
36. Xu J, Lowe RJ, Ivey GN, Jones NL, Brinkan R (2015) Observations of the shelf circulation dynamics along Ningaloo Reef, Western Australia during the austral spring and summer. Cont Shelf Res 95:54–73